Journal of Petroleum Science and Engineering 208 (2022) 109535

Contents lists available at ScienceDirect

Journal of Petroleum Science and Engineering

journal homepage: www.elsevier.com/locate/petrol

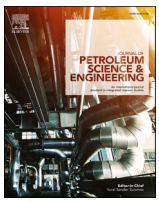

Experimental study on rheological and settling properties of shape memory polymer for fracture sealing in geothermal formations

Abdelmjeed Mohamed [a], Saeed Salehi [a,*], Ramadan Ahmed [a], Guoqiang Li [b]

[a] University of Oklahoma, United States
[b] Louisiana State University, United States

ARTICLE INFO

Keywords:
Lost circulation material
Shape memory polymer
Annular flow
Rheological properties
Wellbore hydraulics
Geothermal drilling

ABSTRACT

This paper studies the rheology and annular flow of a smart lost circulation material (LCM) at 160 °C, using a high-temperature flow loop. The smart LCM is a shape memory polymer (SMP) that activates at high temperatures, and its particle size increases to seal fractures in geothermal formations. SMP was mixed with the base fluid in two different concentrations, 1.0 and 3.0 wt%, to study rheology, wellbore hydraulics, activation process, and settling behavior under different testing conditions.

The results of this study showed that the SMP could be activated at high temperatures. An increase of 80–100% in the particle size was observed at 160 °C. The mud samples showed a high shear-thinning behavior at the two concentrations with a Power-law flow index (n) ranging between 0.025 and 0.101. No additional frictional pressure losses were observed when SMP was added to the base fluid. SMP particles showed an excellent suspension at 1.0 wt% while, at 3.0 wt%, a bed was formed at a low flow rate and without pipe rotation. Increasing the drill pipe rotational speed or flow rate effectively removed the bed and homogeneously dispersed the SMP particles, ensuring a better sealing efficiency. SMP particle dispersion in inclined wells was better than in horizontal wells. Moreover, the findings of this study help optimize the lost circulation treatment by considering a wide range of operating parameters that can further be extended to different systems and geometries.

1. Introduction

Drilling operations in geothermal reservoirs constitute 40–60% of the total cost of geothermal projects, significantly impacting the feasibility of geothermal developments (Bavadiya et al., 2019). The increase in drilling cost is attributed to the extended drilling time due to the high downhole temperature, depth, and nature of geothermal formations (Chemwotei, 2011; Finger and Blankenship, 2010; Kiran and Salehi, 2020; Kruszewski and Wittig, 2018; Olasolo et al., 2016). The high temperature presents formidable challenges to the drilling operations, such as drilling fluid and cement degradation, casing and cement sheath damage, and failure of downhole tools (Shadravan and Amani, 2012; Teodoriu, 2015; Vivas et al., 2020; Wu et al., 2020). The hardness and abrasiveness of geothermal formations prolong the drilling time, wear the drill bit and shorten its life, and increase the vibrations of downhole tools (Baujard et al., 2017; Bavadiya et al., 2017; Finger and Blankenship, 2010; Miyazaki et al., 2019). Moreover, the complex network of natural fractures and narrow mud windows existing in most geothermal reservoirs present many issues to the drilling operation, such as well integrity, loss circulation, and well control problems (Finger and Blankenship, 2010; Kiran and Salehi, 2020; Magzoub et al., 2021; Mohamed et al., 2021a; Shadravan and Amani, 2012; Vollmar et al., 2013).

Lost circulation is one of the problematic events encountered during drilling operations (Alkinani et al., 2019). More than 10% of the nonproductive time was spent on curing lost circulation while drilling in the Gulf of Mexico between 1993 and 2003. In the United States, the cost of lost circulation treatments varies between 10 and 20% of the total geothermal well cost (Lavrov, 2016). Moreover, severe or complete lost circulation may cause a loss in well control, leading to a loss in lives and resources (Magzoub et al., 2021). Lost circulation is more challenging in geothermal wells than oil and gas wells. Several factors contribute to the lost circulation in geothermal wells, such as high downhole temperature, large natural fractures, and low fracture gradients (Lavrov, 2016; Magzoub et al., 2020; Ravi et al., 2006; Tare et al., 2001). Low fracture gradients narrow the mud window that is defined as the operational gap between pore pressure and fracture pressure (Salehi and Nygaard,

* Corresponding author.
E-mail address: salehi@ou.edu (S. Salehi).

https://doi.org/10.1016/j.petrol.2021.109535
Received 20 May 2021; Received in revised form 16 September 2021; Accepted 17 September 2021
Available online 24 September 2021

2011). Narrow mud windows make the pressure control more challenging and increase the possibility of lost circulation events and the number of casings, which, in turn, increase the drilling cost and non-production time (NPT) (Magzoub et al., 2020).

Generally, preventing the losses in the first place is more effective than treating lost circulation (Alsaba, 2015; Magzoub et al., 2020). This can be attained by optimizing drilling fluid formulations, maintain good hole cleaning, and controlling the drilling parameters to optimize wellbore hydraulics. The prior knowledge of downhole conditions and formation stresses and using advanced drilling technologies help mitigate the consequences of lost circulation during drilling operations (Magzoub et al., 2020). However, lost circulation events in the case of a narrow mud window are common because downhole pressure management is difficult. In such cases, drilling engineers and rig crews should be prepared to treat the losses promptly to avoid further complications. This technique is called the corrective method, in which the mud circulation is regained after losses take place (Alsaba, 2015). Several remedy actions can be taken to treat the losses based on the loss type: seepage, severe, or total loss. These techniques can be classified into three main categories: using lost circulation materials (LCMs), LCM pills, and cement squeeze (Wagle et al., 2018).

Various types of lost circulation materials are used to cure fluid losses in geothermal wells. LCMs are mixed with the drilling muds in different concentrations, depending on the loss severity and downhole conditions. Selecting and optimizing the LCM mud formulation is a significant factor in ensuring better treatment results in the field. Mohamed et al. summarized the common lost circulation materials used in drilling operations (Mohamed et al., 2021a). Based on the particle shape, LCMs can be classified into three main categories: granular materials, flakey materials, and fibers. Many laboratory studies were carried out to evaluate the performance of common LCMs under various testing conditions (Akhtarmanesh et al., 2016; Alsaba, 2015; Alsaba et al., 2014; Ezeakacha et al., 2017a, 2017b; Javeri et al., 2011; Lee and Taleghani, 2020; Loeppke et al., 1990; Magzoub et al., 2021; Mansure, 2002). Despite the advancements in LCMs and drilling technologies, more research is still required to overcome the limitations of current lost circulation materials. Sealing complex fracture networks, plugging downhole tools, and formation damage induced by LCMs create serious problems to loss treatments (Magzoub et al., 2021; Mansour et al., 2017). To mitigate the problems, more advanced lost circulation materials were introduced to cure losses under critical downhole conditions, where most conventional LCMs fail. Blends of LCMs, encapsulated pills, nanoparticles (NPs), and shape memory polymers (SMPs) are good examples of these smart LCMs.

One of the recent advancements in the lost circulation material is shape memory polymers (SMPs). They are smart materials that can be programmed to have a temporary deformed shape or size under certain conditions then return to their original form once triggered with an external stimulus (Huang et al., 2005; Lakhera et al., 2012; Meng and Li, 2013). Different mechanisms can trigger shape memory polymers, such as applying light, heat, electricity, moisture, pH, solvent, enzyme, and magnetic field (Fan and Li, 2018; Liu et al., 2009; Mather et al., 2009). Thermal energy is the most common stimulus used with shape memory polymer (Lakhera et al., 2012). The SMP programming cycle starts with heating the polymer to a specific temperature (programming temperature) then deforming its shape by applying external load. Afterward, the polymer is cooled to a temperature lower than the glass transition temperature while the load is still exerted. After removing the load, the deformed shape will be maintained (Fig. 1a). Once the SMP is exposed to a temperature equal to or greater than the programming (activation) temperature, the stored energy will be released to recover the original shape and size, as shown in Fig. 1b (Lakhera et al., 2012; Mather et al., 2009; Yakacki et al., 2007). In addition to this feature, SMPs are inexpensive, easy to process, highly elastic, and have good structural versatility (Liu et al., 2009). These features give SMPs the potential to resolve the loss circulation issues. Since activation can be accurately

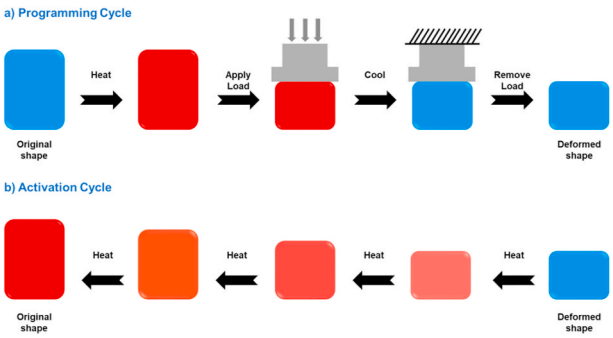

Fig. 1. Programming and activation cycles of thermoset shape memory polymer.

controlled, the risk of plugging downhole drilling tools such as measurement-while-drilling (MWD) and logging tools can be minimized.

Recently, Mansour et al. introduced a novel expandable LCM material to seal fractures and cure fluid losses. Their LCM material is based on a shape memory polymer that can be activated by a temperature of 70 °C. Their method showed promising findings where activated SMP efficiently sealed slot and tapered discs with a high sealing pressure and very low fluid loss. Moreover, the expandable SMP can release a stress of 13 MPa that will help strengthen the wellbore by increasing the hoop stresses around the wellbore (Mansour et al., 2017). Their evaluation was performed only at static conditions using permeability plugging apparatus (PPA), which is not a good representation of the filtration process. Later, they expanded their study to evaluate the SMP performance under dynamic conditions. They demonstrated that the SMP worked much better once mixed with fiber (Mansour et al., 2018). However, the ultimate temperature is limited by SMP melting temperature (120 °C), which is low compared to geothermal formations.

Another study was performed by Magzoub et al., where a new shape memory polymer was evaluated at a high temperature (149 °C) for geothermal drilling applications. To simulate the actual case, they tested the shape memory polymer on artificial aluminum discs and real cylindrical granite cores using a novel flow loop that simulates the sealing efficiency at dynamic conditions. Their method and new apparatus are well described in their published work (Magzoub et al., 2021). Their analysis showed that SMP could be an excellent candidate to seal large fractures in geothermal formations with additional wellbore strengthening features. They also confirmed the findings of Mansour et al. that combining SMP with fiber provides better sealing efficiency.

For a successful application, many parameters should be considered before treating the lost circulation. These parameters include formation type, lithology, and mud properties such as pH, alkalinity, rheological properties, and LCM type and concentration. Optimizing the mud formulation is as vital as selecting the LCM to ensure successful treatments (Magzoub et al., 2021). For instance, rheological properties play a crucial role in loss prevention and treatment. Rheological properties significantly impact wellbore hydraulics and fluid capability to transport LCM particles. Loss prevention is primarily achieved by controlling wellbore hydraulics, particularly the equivalent circulating density (ECD). The uncontrolled increase in ECD may induce fractures in the drilled formation when it exceeds the fracturing pressure, increasing the fluid losses and complicating the drilling operation (Wastu et al., 2019). Moreover, the sealing efficiency is highly impacted by LCM dispersion into the mud. The previous studies on SMP focused only on evaluating the sealing efficiency of SMP on a small laboratory scale without studying the SMP transportation and its impact on fluid rheology and hydraulics. Therefore, this work aims to study SMP transportation and evaluate its effect on mud rheology and wellbore hydraulics at high temperatures using a large-scale flow loop. Additionally, a wide range of operating parameters was considered in this work, such as flow rate,

inclination, and pipe rotational speed, to optimize the lost circulation treatment. In the following sections, the material and method used to conduct this study are described. The findings and observations are then discussed, and finally, the main conclusions of this study are summarized.

2. Materials and methods

2.1. Materials

Several 0.04-m^3 (10.5-gallon) fluid samples were prepared in the laboratory to conduct this study. Fresh tap water was used as the base fluid, while THERMA-VIS was added to provide the required viscosity to suspend and carry the LCM particles. THERMA-VIS is a commercial additive obtained from a service company. It is a synthetic hectorite clay developed to activate and build viscosity at a high temperature, above 149 °C (Mohamed et al., 2021a, 2021b, 2021b). It has a specific gravity of 1.0 and thermal stability of up to 370 °C (Baroid, 2012). THERMA-VIS was used with the base fluid due to its high thermal resistance and clear appearance, allowing flow visualization. A smart LCM was evaluated to investigate its effect on mud rheology and wellbore hydraulics. The smart LCM is a thermoset shape memory polymer (SMP) programmed to activate downhole at temperatures above 149 °C. Once the SMP is thermally activated, the particle size increases to gain its original shape and size, which helps seal the large fractures in geothermal formations. The used SMP has a density of 950 kg/m^3 (59.3 lb/ft^3) and a particle size ranging between 840 and 2360 μm.

The particle size distribution of the shape memory polymer was obtained using dry sieve analysis due to the limitation of the particle size analyzer, which cannot measure particles larger than 2000 μm to ensure more accurate results that even large particles are included. A sample of 200 g was sieved using a sieve shaker that consists of various sieve trays ranging between 53 and 2360 μm. Most SMP particles were larger than 500 μm, where 84.9 wt% of SMP particles ranged between 840 and 2360 μm and 5.9 wt% of the particles were greater than 2360 μm. As shown in Fig. 2, SMP exhibited a median particle size (D_{50}) of about 1400 μm.

2.2. Methods

2.2.1. Flow loop experiments

A high-temperature flow loop (Fig. 3) was built to study the effect of SMP concentration on rheology, wellbore hydraulics, and SMP settling behavior. The flow loop consists of five main sections; i) A heating system is added to the setup to heat the mud to the desired temperature. An oil pump circulates the heating oil through an electric heater, then to a coil inside the mud tank, where the heat transfer occurs before the relatively cold oil returns to the oil tank. The heating oil is circulated inside the mud tank through a heating coil to avoid mud contamination. ii) Circulation system that consists mainly of two pumps to circulate the oil and mud. iii) 10-feet horizontal pipe viscometer to study the rheological behavior and wellbore hydraulics. iv) The main test section consists of a 10-feet long concentric annulus (2.067″ × 1″) with two viewports and a motor to rotate the inner pipe. The viewports are installed to visualize the annular flow of SMP mud. The test section position can be adjusted to different inclination angles to simulate horizontal and inclined wells. The inclination is changed by lifting the outlet side using an overhead crane, while safety pins are added to the setup to secure the test section at the desired inclination angle. v) Data acquisition and control system is used to obtain and record the measurement data and controls the setup components. This system consists of a computer, data acquisition (DAQ) card, variable frequency drives (VFD), temperature and pressure sensors, and a flow meter.

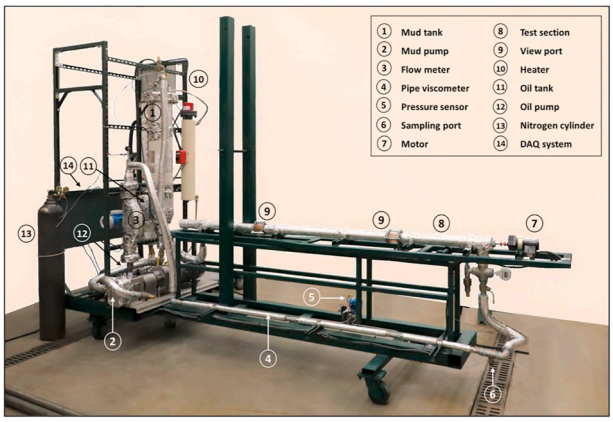

Fig. 3. High-temperature flow loop used in this study.

For every experiment, a 0.04-m^3 (10.5-gallon) fluid sample was prepared in the mud tank. The rheological behavior of the fluid was studied at different temperatures, 21–160 °C. The pressure drops across the pipe viscometer and flow rates were recorded using a data acquisition system. This data is then analyzed to determine the rheological properties of the mud samples. The flow loop is developed to study the annular flow of SMP muds at a wide range of parameters such as temperature, SMP concentration, inclination angle, flow rate, and drill pipe rotational speed. The visualization data acquired by the high-speed camera is processed and used to investigate the transport efficiency, settling behavior, and SMP activation process. SMP is added to the base fluid at a high temperature (149 °C) after the viscosifier activates and builds enough viscosity to suspend the SMP particles. The experiment is started when the desired fluid temperature reaches the testing temperature. Table 1 describes the experimental parameters used in flow loop experiments.

2.2.2. Rheological analysis calculations

The pressure drops and flow rate data obtained from the flow loop are analyzed to determine the rheology model that describes the base mud and SMP mud. The following procedure is followed to obtain the

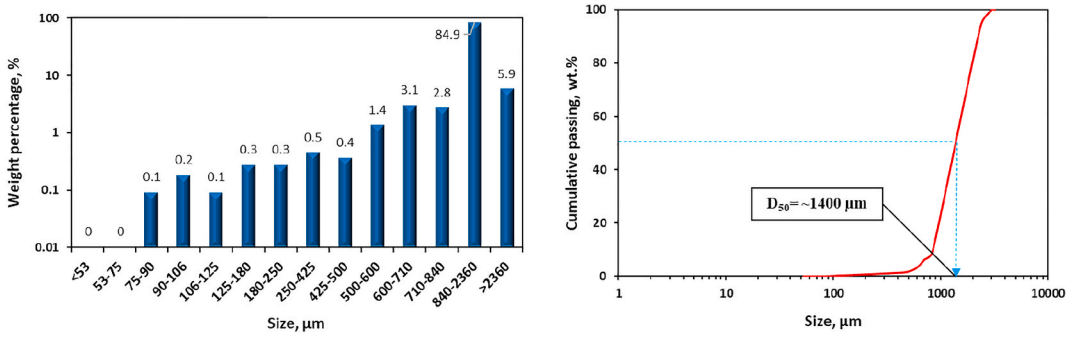

Fig. 2. The particle size distribution of shape memory polymer used in this study.

Table 1
Experimental parameters for flow loop experiments.

Parameter	Range
SMP concentration	0, 1.0, and 3.0 wt%
Temperature	21–160 °C
Pressure	689.5 KPa (100 psi)
Inclination angle (from vertical)	90°, 67.5°, and 45°
Flow rate	6.3×10^{-5}-1.26×10^{-3} m^3/s (1–20 gpm)
Pipe rotational speed	0, 75, and 150 RPM

corrected flow curve for each fluid sample:

i. The flow rate (Q) and differential pressure (ΔP) data, obtained from the flow meter and pipe viscometer, are converted from gallon per minute (gpm) and inch water (in H_2O) to cubic meter per second (m^3/s) and pascal (Pa).
ii. Q and ΔP data are converted to wall shear stress (τ_w) and nominal Newtonian wall shear rate ($\dot{\gamma}_{nom}$) using the viscometer diameter (D = 0.02286 m) and length (L = 0.9144 m) by applying Eqs (1) and (2).

$$\tau_w = \frac{D\Delta P}{4\,L} \tag{1}$$

$$\dot{\gamma}_{nom} = \frac{8V}{D} \tag{2}$$

iii. τ_w and $\dot{\gamma}_{nom}$ data are plotted in a logarithmic scale and fitted with a straight line to check for the Power-law model's applicability. The consistency (K) and flow index (n) are obtained from the curve fitting. K corresponds to the intercept with the y-axis, while n is the slope of the straight line.
iv. Fluid properties and n data are used to plot the laminar flow limit line and check the laminar flow for all the data points. The points laying on or to the right of the laminar flow limit line correspond to the turbulent flow. The turbulent flow data must be excluded from the analysis. Equation (3) is used to plot the laminar flow limit line for power-law fluids (Alderman and Pugh, 2004). To validate the results, another method is used to check for laminar flow by calculating Fanning friction factor (f) and the generalized Reynolds number (*Re*) for laminar and turbulent flow data, as shown in Equations (4)–(6). After plotting the Fanning friction factor against the generalized Reynolds number in a log-log scale, the transition from laminar to turbulent is detected when the points deviate from the straight line.

$$\tau_c = \frac{\rho D^2}{8}\left[\frac{n}{404}\frac{\left(\frac{1+3n}{4n}\right)}{(n+2)\left(\frac{n+2}{n+1}\right)}\right]\left[\frac{8V}{D}\right]^2 \tag{3}$$

$$f = \frac{\tau_w}{1/2\,\rho v^2} \tag{4}$$

$$Re = \frac{8\rho\bar{v}^2}{K\dot{\gamma}_w^n} \tag{5}$$

where,

$$\dot{\gamma}_w = \frac{3n+1}{4n}\dot{\gamma}_{nom} \tag{6}$$

v. The calculations do not consider the correction for the end effect because the pipe viscometer was designed to account for the end effect. The measurements are taken after 1.2 m from the inlet and before 0.9 m from the outlet of the pipe viscometer. Therefore, the measured data will not be affected by the two ends.
vi. After excluding the turbulent data, τ_w is plotted against $\dot{\gamma}_{nom}$ in a logarithmic scale. The curve is fitted, and the correct K and n are obtained from the curve fitting as discussed in step (iii). K and n are used to construct the flow curve for each fluid sample by calculating the shear stress (τ) at different shear rates ($\dot{\gamma}$) using the Power-law model (Equation (7)). The flow curve is constructed for shear rate values ranging from 0.1 to 1000 1/s.

$$\tau = K\dot{\gamma}^n \tag{7}$$

vii. K and n are used to calculate the apparent viscosity at different shear rates to compare the performance of different fluid samples. Apparent viscosity is calculated using Equation (8).

$$\mu_a = K\dot{\gamma}^{n-1} \tag{8}$$

3. Results, observations, and discussions

3.1. Rheology experiments

3.1.1. Effect of temperature on the base fluid

First, the rheological properties of the base fluid were measured at different temperatures (21, 93, and 160 °C) to study its performance and then investigate the effect of SMP on its rheological behavior. Following the procedure illustrated in steps from i to vii, the flow curve of the base fluid at different temperatures was construed in Fig. 4a. It was observed from the flow curve that the base fluid is a non-Newtonian fluid with shear-thinning behavior at all testing temperatures. The thinning degree varied with temperature because the used viscosifier (synthetic hectorite clay) is engineered to activate and build viscosity with high shear-thinning behavior at high temperatures (Mohamed et al., 2021a, 2021b, 2021b). The power-law model can describe the base fluid behavior with a correlation parameter (R^2) and root-mean-square error (RMSE) of 0.88–0.93 and 0.04–0.12, respectively. The power-law model is a simple and suitable model to describe shear-thinning fluids (Mohamed et al., 2021a; Wu, 2016). Casson and Herschel–Bulkley models were also considered in the rheological analysis. The Casson model yielded a correlation parameter of around 0.86, which is slightly lower than the power-law model. Because the base drilling fluid exhibited a low yield stress (τ_0) value of about 0.18 Pa, no significant change in the rheological behavior of the drilling fluid was observed. A slight improvement in the flow curve was noticed with an R^2 of 0.882–0.931. Therefore, the drilling fluid can be well described by both power-law and Herschel–Bulkley models.

As shown in Fig. 4a, the degree of thinning increases with temperature, which can be proven from the flow index values (n). The base fluid showed a flow index of 0.454, 0.168, and 0.101 at 21, 93, and 160 °C, respectively. However, higher viscosities were observed at high temperatures due to the thermally induced activation of the synthetic hectorite clay, improving the mud capacity of carrying/suspending the LCM and drilled cuttings (Baroid, 2012; Mohamed et al., 2021b). The drop in the apparent viscosity with the increase in shear rate also confirmed the high shear-thinning behavior of the base fluid, Fig. 4b. This high shear-thinning performance is favorable in drilling operations because it makes the frictional pressure drops less sensitive to the change in flow rate. Therefore, less frictional pressure drops would result during mud circulation through bit nozzles and tubular systems than other fluid systems with shear-thickening behavior or a lower degree of shear-thinning.

3.1.2. Effect of shape memory polymer (SMP)

The shape memory polymer was added to the base fluid in two concentrations, 1.0 and 3.0 wt%. The rheology data were analyzed for each fluid sample using the procedure discussed earlier. τ_w and $\dot{\gamma}_{nom}$ data of the SMP mud samples yielded a straight line in a logarithmic scale

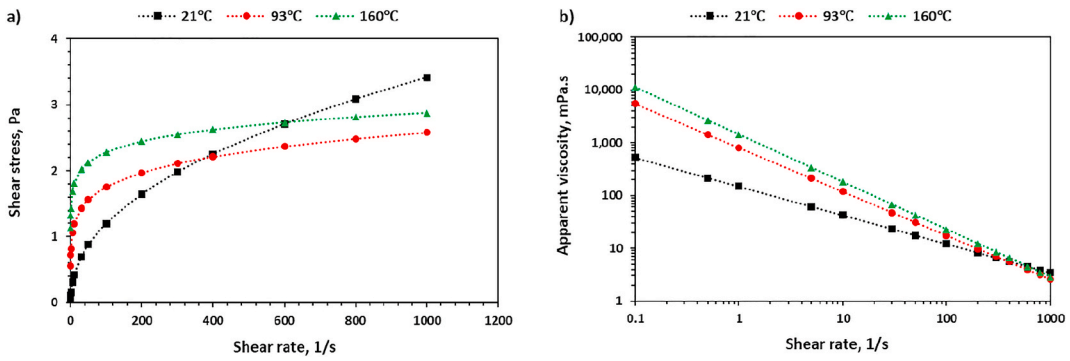

Fig. 4. Effect of temperature on the base fluid's performance: a) flow curve, and b) apparent viscosity.

with an R-squared and RMSE ranging between 0.93-0.97 and 0.007–0.01, respectively. Similar to the base fluid, SMP mud exhibited low yield stress values (≈0.2 Pa); therefore, the flow behavior of SMP mud can be well described by both Power-law and Herschel–Bulkley models. K and n values were obtained from the curve fitting and used to construct the corrected flow curves at 160 °C after excluding the turbulent flow points. A high shear-thinning behavior ($n < 1$) was observed with SMP mud at both concentrations, as shown in Fig. 5a. The flow index (n) decreased from 0.101 to 0.061 and 0.025 as SMP concentration increased from 0 to 1.0 and 3.0 wt%, respectively, presenting a slightly higher thinning degree than the base fluid. The apparent viscosity is calculated from the pipe viscometer data measured at 160 °C. The viscosity profile confirmed the shear-thinning behavior of all mud samples, where the apparent viscosity decreased with the shear rate, as shown in Fig. 5b. However, a slightly lower apparent viscosity resulted in SMP mud at high shear rates. The decrease in apparent viscosity can be attributed to the presence of SMP particles in the suspension that increased the shearing on the base fluid. The increased viscosity at low shear rates prevailing in the annulus would yield a better hole cleaning, while the lower viscosity at high shear rates present in the drill pipe would minimize the pumping pressure; thus, no increase in ECD will result (Caenn et al., 2017). The pressure drop profile also confirmed the high shear-thinning behavior of SMP mud at 160 °C (Fig. 6a). In the laminar flow regime, 1.0 wt% SMP reduced frictional pressure drops with around 120 Pa while the mud sample containing 3.0 wt% SMP showed a similar performance to the base fluid. The friction factor is presented in Fig. 6b as a function of the generalized Reynolds number. The flow regime changed from laminar to turbulent flow when the generalized Reynolds number reached around 4000. A slight reduction in the frictional pressure drops was observed with 3.0 wt% SMP in the turbulent flow regime. This reduction can help avoid the increase in ECD that may complicate the lost circulation treatment and cause additional losses if it exceeds the fracture pressure of the drilled formation.

3.2. Shape memory polymer activation

The shape memory polymer was used in this study as a smart lost circulation material programmed to activate at a high temperature (above 149 °C). The activation process was studied by visualizing the annular flow through two viewports with the aid of a high-speed camera. The experiments were performed at 21 °C and 160 °C to detect the change in SMP particles with temperature. The captured videos were processed and analyzed using frame-by-frame image processing techniques with the aid of commercial image processing software. Fig. 7 shows the activation process of SMP particles with temperature. In this part, SMP was added to the base fluid in 1.0 wt% to spot the particles easily. Initially, SMP particles have an irregular shape with a particle size ranging from 840 to 2360 μm (0.84–2.36 mm). At low temperature (21 °C), most SMP particles were ranging from 1 to 2 mm (Fig. 7a), while a significant increase in the SMP particle size was observed at high temperature (160 °C). The SMP particle size reached up to 3–5 mm with some small particles (Fig. 7b). The activation of thermoset shape memory polymers was addressed in previous studies by visualizing the change in particle size before and after heating (Mansour et al., 2018, 2019), infrared laser light (Leng et al., 2010), or by tracking the change in energy (stresses and strains) during the programming and activation processes (Fan and Li, 2018; Li and Xu, 2011). However, the increase in particle size observed in this study confirmed the thermally induced activation of the shape memory polymer at high temperatures within the mud system, considering the effect of other mud additives and mud circulation. This particular reason makes the results of this study more representative of actual field operations, while previous studies considered only the temperature effect in the absence of other effects.

Based on these observations, the shape memory polymer can be programmed to activate at a specific temperature after reaching the targeted formation to seal large fractures with minimal risk of plugging downhole equipment, such as MWD and logging tools. As reported in previous studies, these size variations would be more efficient in bridging and sealing fractures (Alsaba, 2015; Alsaba et al., 2017;

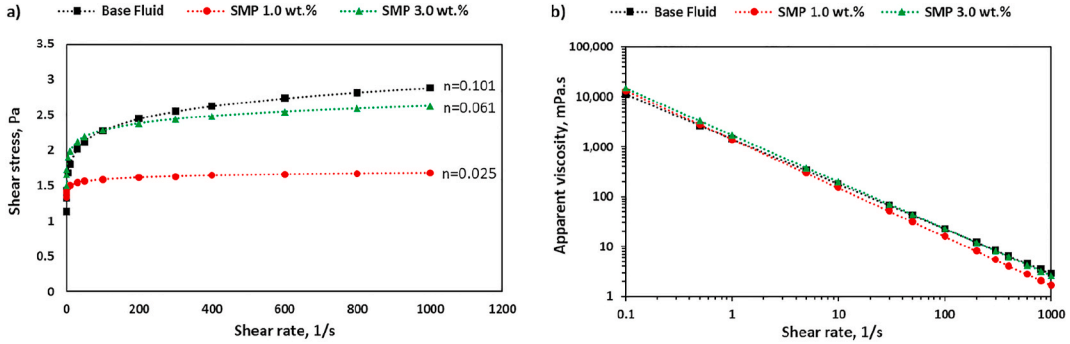

Fig. 5. Effect of SMP concentration on rheological properties at 160 °C: a) flow curve, and b) apparent viscosity.

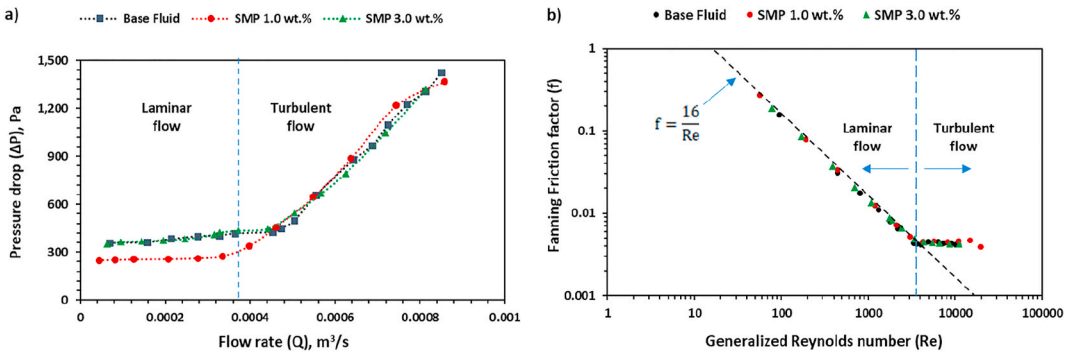

Fig. 6. Effect of SMP concentration on frictional pressure drops at 160 °C.

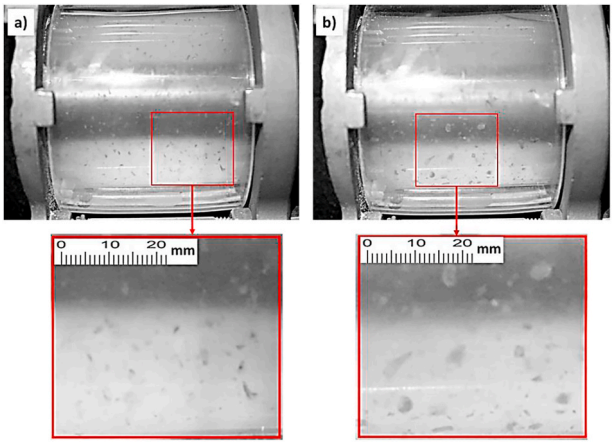

Fig. 7. Effect of temperature on SMP particles: a) 21 °C, and b) 160 °C. A clear increase in particle size is seen at the temperature of 160 °C.

Ezeakacha et al., 2017b; Magzoub et al., 2020; Whitfill, 2008). Large particles are required to form the bridge on the fracture, while small particles help create the seal matrix and plug the space between large particles and the fracture wall (Magzoub et al., 2021).

3.3. Effect of test variables on SMP dispersion

In this section, a series of experiments were performed to study the parameters affecting the SMP particles dispersion in the annulus at a high temperature, 160 °C. The experimental parameters considered in this part are SMP concentration, pipe rotational speed, flow rate, and inclination angle. The ranges of experimental parameters were described in Table 1. The visualization data was processed and analyzed to detect solid particles settlement and identify the optimum parameters for better SMP dispersion, thus, better sealing efficiency. The shape memory polymer was added to the base fluid in two concentrations, 1.0 and 3.0 wt%. First, the impact of pipe rotational speed and flow rate was evaluated at the horizontal angle, representing the worst case. The inclination angle effect was then studied on both concentrations.

3.3.1. Effect of flow rate

At 1.0 wt%, the SMP particles were homogeneously distributed in the annulus at a low flow rate of 0.00013 m^3/s (2 gpm). This flow rate corresponds to an average annular velocity of 0.083 m/s (16.33 ft/min). As shown in Fig. 8, no settlement was observed with SMP particles at this low annular velocity, and the pipe rotation was unnecessary while circulating 1.0 wt% SMP mud. This behavior was also observed at higher flow rates because the increased annular velocity dispersed the particles and subsequently improved mud carrying capacity (Werner, 2018). Therefore, increasing the flow rate with low SMP concentrations is not required. The increased flow rate would add more frictional pressure drops and consequently increase the ECD. The uncontrolled increase in ECD may induce fractures in the drilled formation when it exceeds the fracturing pressure, increasing the fluid losses and complicating the drilling operation (Wastu et al., 2019).

3.3.2. Effects of SMP concentration and pipe rotation

When the SMP concentration was increased from 1% to 3% by weight at a low flow rate, 0.00013 m^3/s (2 gpm), moving and stationary beds were formed in the horizontal annulus. The bed thickness was high, covering almost 40% of the cross-sectional area of the annulus, as shown in Fig. 9a. These deposited particles can reduce the sealing efficiency of the SMP and cause pipe sticking and difficulties in the casing and liner placement (Boyou et al., 2019). However, increasing the flow rate to 0.00032 m^3/s (5 gpm) helped erode the beds and significantly improved the carrying capacity of the fluid and the dispersion of SMP particles (Fig. 9d). Similarly, the pipe rotation was very effective in agitating and eroding the bed, enhancing the SMP particles dispersion, especially at low flow rates (Fig. 9b and c). Increasing the pipe rotational speed to 75 RPM was adequate to prevent bed formation, as shown in Fig. 9b. Therefore, an adequate level of annular velocity or pipe rotational speed should be maintained in horizontal wells to ensure the dispersion of SMP and maintain the sealing efficiency of the mud containing 3.0 wt% SMP.

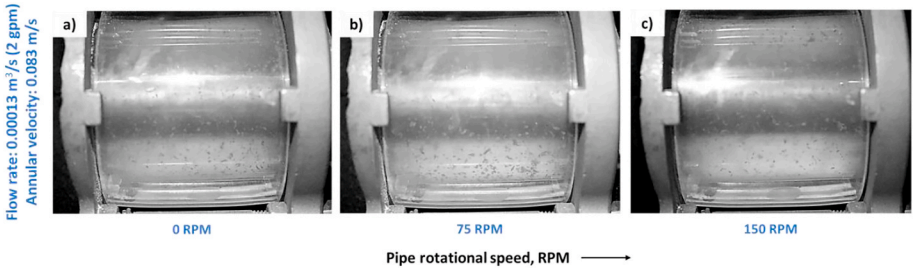

Fig. 8. Effect of pipe rotational speed on SMP particles dispersion at the horizontal angle, 1.0 wt% concentration, and low flow rate: 0.000126 m^3/s (2 gpm)- 160 °C.

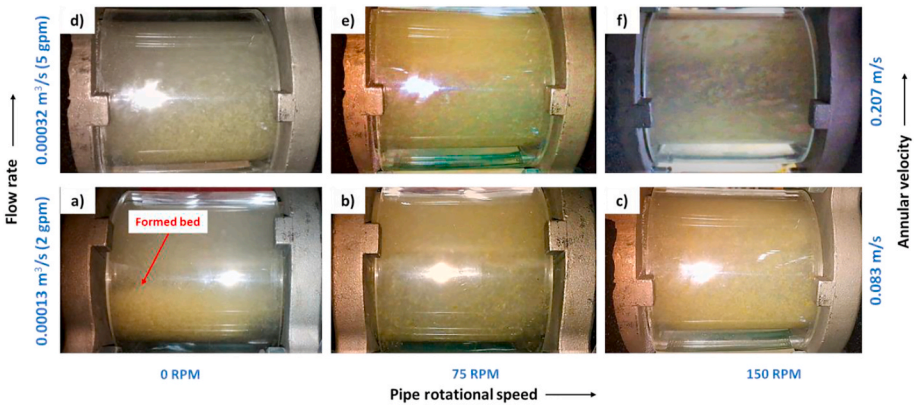

Fig. 9. Effect of pipe rotational speed and flow rate/annular velocity on SMP particles dispersion at the horizontal angle, and 3.0 wt% concentration- 160 °C.

3.3.3. *Effect of inclination*

Fig. 10 compares the SMP mud performance at various concentrations (1.0 and 3.0 wt%) and inclination angles (90°, 67.5°, and 45° from vertical). At 1.0 wt% SMP concentration, the inclination angle had no impact on SMP particle dispersion. SMP particles were homogeneously distributed in the annular space at all inclination angles, as shown in Fig. 10a-c. On the other hand, when the concentration was increased to 3.0 wt% and without pipe rotation, the SMP mud performed better at lower inclination angles (from vertical) in terms of transport efficiency and particle dispersion. A high thickness bed was formed at a horizontal angle (Fig. 10d). While, under the same pipe rotation and flow rate conditions, the SMP particles were asymmetrically suspended at a 67.5° inclination angle and symmetrically suspended at a 45° inclination angle from vertical (Fig. 10e and f). Therefore, the SMP transportation in horizontal wells is more critical and challenging than inclined and vertical wells because, in horizontal wells, the vertical component of fluid velocity acting on SMP particles is equal to zero. Thus, solid particles tend to settle down easily with the limited hydrodynamic force that opposes the gravitational force and prevents deposition (Czuprat et al., 2020). Deposited SMP particles form unconsolidated beds in which the particles travel by rolling (Mahmoud et al., 2020). The settling behavior is a complex phenomenon, and many parameters should be considered to understand it well, including the shape, size, and density of solid particles. Fig. 11 summarizes the effect of test parameters on the SMP dispersion to determine the optimum conditions for SMP transport at the two concentrations.

The results of this study were obtained using a large-scale laboratory setup with dimensions smaller than actual field dimensions; therefore, as future work, a computational fluid dynamic study will be performed to upscale the experimental results to other systems with different geometries and sizes to optimize the operating parameters of the lost circulation treatment such as pipe rotational speed and flow rate.

4. Conclusions

An experimental study was conducted using a large-scale flow loop to evaluate the effect of shape memory polymer on rheology and wellbore hydraulics at high-temperature conditions. Viewports were installed on the test section to visualize the flow with the aid of a high-speed camera to study the transport efficiency and SMP distribution under a wide range of test parameters. The experiments were conducted by varying SMP concentrations, inclination angle, pipe rotational speed, and flow rate. Based on the results, the following conclusions can be drawn:

- The base fluid used in this study to carry and suspend the SMP particles is a non-Newtonian fluid with a strong shear-thinning behavior that fits the Power-law model. The viscosifier used with the base fluid is a synthetic hectorite clay that activates and builds viscosity at high temperatures. The viscosity increases with temperature to reach the maximum viscosity at around 150 °C due to the thermally induced activation.
- Adding the smart lost circulation materials, with a concentration up to 3.0 wt%, increased the degree of shear-thinning. The Power law model could well describe all SMP mud samples. The viscosity profile of SMP mud was similar to that of the base fluid. SMP mud exhibited a slightly lower apparent viscosity due to the presence of SMP particles in the suspension.

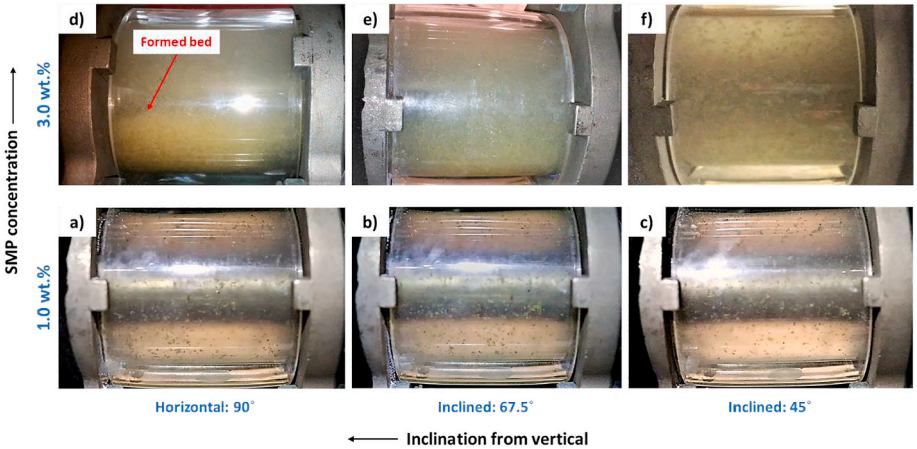

Fig. 10. Effect of inclination angle and concentration on SMP particles dispersion at low flow rate: 0.000126 m^3/s (2 gpm), without pipe rotation- 160 °C.

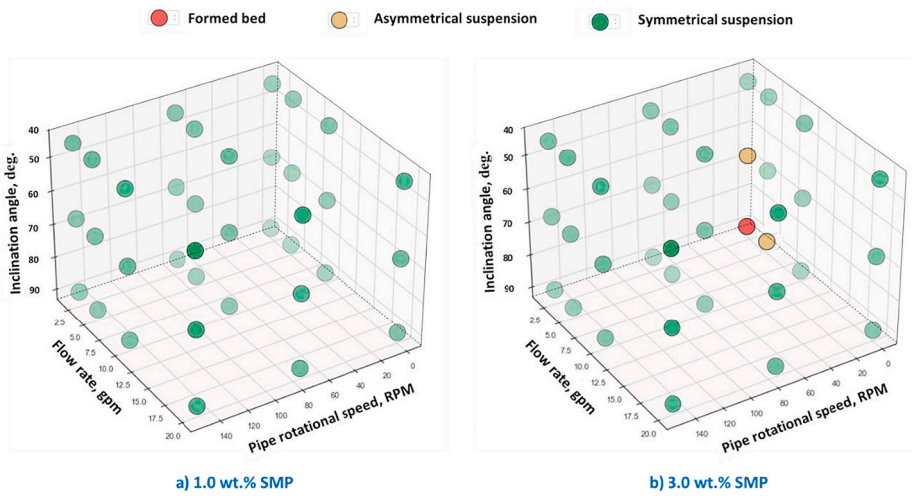

Fig. 11. Effect of inclination angle, flow rate, and pipe rotation on SMP particles transport at 160 °C.

- The SMP particle size increased from 1 to 2 to 3–5 mm when the temperature increased from room temperature (21 °C) to 160 °C, proving the induced activation of SMP at high temperatures (above 149 °C). The increase in particle size confirmed that SMP has the potential to efficiently seal large fractures and treat lost circulation with minimal risk of plugging downhole tools. However, further research should be conducted to evaluate the sealing efficiency of the shape memory polymer at diverse conditions in the existence of fractured mediums.
- The SMP dispersion was studied by visualizing the annular flow under different experimental parameters such as SMP concentration, pipe rotation, flow rate, and inclination angle. The transport efficiency varied significantly with these parameters. It was observed that, at low concentration (1.0 wt%), SMP particles were transported efficiently without forming a stationary or moving bed at all testing conditions. Thus, transporting SMP with 1.0 wt% is not problematic, and increasing the pipe rotational speed and/or flow rate was not required.
- At 3.0 wt% concentration, the SMP mud performed better in inclined configurations while a bed was formed in the horizontal test section. The flow rate and pipe rotation improved the transport efficiency of SMP mud significantly. Maintaining a minimum annular velocity of 0.207 m/s (40.81 ft/min) or a minimum pipe rotational speed of 75 RPM was required in horizontal inclination to ensure better dispersion of SMP particles.

Credit author statement

Abdelmjeed Mohamed: Methodology, Formal analysis, Investigation, Data curation, Writing – original draft, Writing – review & editing, Visualization. **Saeed Salehi:** Conceptualization, Methodology, Resources, Data curation, Writing – review & editing, Supervision, Project administration, Funding acquisition. **Ramadan Ahmed:** Conceptualization, Methodology, Resources, Data curation, Writing – review & editing, Supervision, Project administration. **Guoqiang Li:** Conceptualization, Resources, Writing – review & editing, Funding acquisition.

Declaration of competing interest

The authors declare that they have no known competing financial interests or personal relationships that could have appeared to influence the work reported in this paper.

Acknowledgment

The authors would like to acknowledge the U.S. Department of Energy Office of Energy Efficiency and Renewable Energy (EERE) under the Geothermal Program Office Award Number DE-EE0008602 for funding this research.

Nomenclature

Acronyms

DAQ	data acquisition
ECD	equivalent circulating density
LCM	lost circulation material
MWD	measurement-while-drilling
NPs	nanoparticles
NPT	non-productive time
PPT	permeability plugging test
RMSE	root-mean-square error
SMP	shape memory polymer
VFD	variable frequency drive

Symbols

$\bar{v}$	: average velocity
$\dot{\gamma}_{nom}$	: nominal wall shear rate, 1/s
μ_a	: apparent viscosity, mPa.s or cP

τ_c	: critical wall shear stress, Pa
τ_w	: wall shear stress, Pa
D	diameter, m
gpm	gallon per minute
K	consistency, Pa.s^n or equivalent cP
L:	length, m
n	flow index, dimensionless
Q	flow rate, m^3/s
Re	Reynold's number, dimensionless
V	velocity, m/s
γ	: Shear rate, 1/s
ΔP	frictional pressure drops, Pa
μ	: viscosity, Pa.s
ρ	: density, kg/m^3
τ	: shear stress, Pa

References

Akhtarmanesh, S., Al-Saba, M., Cedola, A.E., Qader, R., Caldarola, V.T., Hareland, G., Nygaard, R., 2016. Barite nano-micro particles with LCM seals fractured form better in weighted water based drilling fluids. In: The 50th US Rock Mechanics/Geomechanics Symposium 2016. OnePetro, Houston, Texas, USA, pp. 1590–1595.

Alderman, N.J., Pugh, S.J., 2004. Non-Newtonian Fluids: Tube Viscometry – Worked Example (No. 04005), the ESDU Series on Internal Flow. London, United Kingdom.

Alkinani, H.H., Al-Hameedi, A.T.T., Dunn-Norman, S., Al-Alwani, M.A., Mutar, R.A., Al-Bazzaz, W.H., 2019. State-of-the-art review of lost circulation materials and treatments - Part I: general trends and uses. In: Abu Dhabi International Petroleum Exhibition and Conference 2019, ADIP 2019. Society of Petroleum Engineers, Abu Dhabi, UAE. https://doi.org/10.2118/197393-ms.

Alsaba, M., 2015. Investigation of Lost Circulation Materials Impact on Fracture Gradient. Dr. Diss. Missouri University of Science and Technology.

Alsaba, M., Al Dushaishi, M.F., Nygaard, R., Nes, O.M., Saasen, A., 2017. Updated criterion to select particle size distribution of lost circulation materials for an effective fracture sealing. J. Petrol. Sci. Eng. 149, 641–648. https://doi.org/10.1016/j.petrol.2016.10.027.

Alsaba, M., Nygaard, R., Saasen, A., Nes, O.M., 2014. Laboratory evaluation of sealing wide fractures using conventional lost circulation materials. Proc. - SPE Annu. Tech. Conf. Exhib. 1, 1–18. https://doi.org/10.2118/170576-ms.

Baroid, 2012. Product Data Sheets.

Baujard, C., Hehn, R., Genter, A., Teza, D., Baumgartner, J., Guinot, F., Martin, A., Steinlechner, S., 2017. Rate of penetration of geothermal wells: a key challenge in hard rocks. In: The 42nd Workshop on Geothermal Reservoir Engineering. Stanford, California, USA.

Bavadiya, V., Srivastava, S., Salehi, S., Teodoriu, C., 2019. Geothermal drilling training and Certification : should it Be Different ?. In: The 44th Workshop on Geothermal Reservoir Engineering. Stanford, California, USA.

Bavadiya, V.A., Alsaihati, Z., Ahmed, R., Gustafson, K., 2017. Experimental investigation of the effects of rotational speed and weight on bit on drillstring vibrations, torque and rate of penetration. In: The SPE Abu Dhabi International Petroleum Exhibition and Conference. Abu Dhabi, UAE. https://doi.org/10.2118/188427-ms.

Boyou, N.V., Ismail, I., Wan Sulaiman, W.R., Sharifi Haddad, A., Husein, N., Hui, H.T., Nadaraja, K., 2019. Experimental investigation of hole cleaning in directional drilling by using nano-enhanced water-based drilling fluids. J. Petrol. Sci. Eng. 176, 220–231. https://doi.org/10.1016/j.petrol.2019.01.063.

Caenn, R., Darley, H.C.H., Gray, G.R., 2017. Composition and properties of drilling and completion fluids: seventh ed., seventh ed. In: Composition and Properties of Drilling and Completion Fluids, seventh ed. Elsevier. https://doi.org/10.1016/C2015-0-04159-4.

Chemwotei, S.C., 2011. Geothermal Drilling Fluids.

Czuprat, O., Faugstad, A.M., Byrski, P., Schulze, K., 2020. Hole cleaning efficiency of sweeping pills in horizontal wells - facts or philosophy?. In: SPE Annual Technical Conference and Exhibition. Society of Petroleum Engineers (SPE). https://doi.org/10.2118/201634-ms.

Ezeakacha, Chinedum Peter, Salehi, S., Bi, H., 2017a. How does rock type and lithology affect drilling fluid's filtration and plastering?. In: The AADE National Technical Conference and Exhibition. Houston, Texas, USA.

Ezeakacha, C.P., Salehi, S., Hayatdavoudi, A., 2017b. Experimental study of drilling fluid's filtration and mud cake evolution in sandstone formations. J. Energy Resour. Technol. 139 https://doi.org/10.1115/1.4035425.

Fan, J., Li, G., 2018. High enthalpy storage thermoset network with giant stress and energy output in rubbery state. Nat. Commun. 9 https://doi.org/10.1038/s41467-018-03094-2.

Finger, J., Blankenship, D., 2010. Handbook of Best Practices for Geothermal Drilling, Sandia Report.

Huang, W.M., Yang, B., An, L., Li, C., Chan, Y.S., 2005. Water-driven programmable polyurethane shape memory polymer: demonstration and mechanism. Appl. Phys. Lett. 86, 1–3. https://doi.org/10.1063/1.1880448.

Javeri, S.M., Haindade, Z.W., Jere, C.B., 2011. Mitigating loss circulation and differential sticking problems using silicon nanoparticles. In: Proceedings of the SPE/IADC Middle East Drilling Technology Conference and Exhibition, pp. 136–139. https://doi.org/10.2118/145840-ms.

Kiran, R., Salehi, S., 2020. Assessing the relation between petrophysical and operational parameters in geothermal Wells : a machine learning approach. In: Proceedings of 45th Workshop on Geothermal Reservoir Engineering. Stanford, California, USA.

Kruszewski, M., Wittig, V., 2018. Review of failure modes in supercritical geothermal drilling projects. Geoth. Energy 6, 1–29. https://doi.org/10.1186/s40517-018-0113-4.

Lakhera, N., Laursen, C.M., Safranski, D.L., Frick, C.P., 2012. Biodegradable thermoset shape-memory polymer developed from poly(β-amino ester) networks. J. Polym. Sci., Part B: Polym. Phys. 50, 777–789. https://doi.org/10.1002/polb.23059.

Lavrov, A., 2016. Lost Circulation: Mechanisms and Solutions, Lost Circulation: Mechanisms and Solutions. Gulf Professional Publishing, Oxford, UK. https://doi.org/10.1016/C2015-0-00926-1.

Lee, L., Taleghani, A.D., 2020. The effect particle size distribution of granular LCM on fracture sealing capability. In: The SPE Annual Technical Conference and Exhibition. Society of Petroleum Engineers. https://doi.org/10.2118/201668-ms. Virtual.

Leng, J., Zhang, D., Liu, Y., Yu, K., Lan, X., 2010. Study on the activation of styrene-based shape memory polymer by medium-infrared laser light. Appl. Phys. Lett. 96, 2008–2011. https://doi.org/10.1063/1.3353970.

Li, G., Xu, W., 2011. Thermomechanical behavior of thermoset shape memory polymer programmed by cold-compression: testing and constitutive modeling. J. Mech. Phys. Solid. 59, 1231–1250. https://doi.org/10.1016/j.jmps.2011.03.001.

Liu, Y., Lv, H., Lan, X., Leng, J., Du, S., 2009. Review of electro-active shape-memory polymer composite. Compos. Sci. Technol. 69, 2064–2068. https://doi.org/10.1016/j.compscitech.2008.08.016.

Loeppke, G.E., Glowka, D.A., Wright, E.K., 1990. Design and evaluation of lost-circulation materials for severe environments. JPT, J. Pet. Technol. 42, 328–337. https://doi.org/10.2118/18022-PA.

Magzoub, M., Salehi, S., Li, G., Fan, J., Teodoriu, C., 2021. Loss circulation prevention in geothermal drilling by shape memory polymer. Geothermics 89, 101943. https://doi.org/10.1016/j.geothermics.2020.101943.

Magzoub, M.I., Salehi, S., Hussein, I., Nasser, M., 2021. Development of a polyacrylamide-based mud formulation for loss circulation treatments. J. Energy Resour. Technol. 143, 1–8. https://doi.org/10.1115/1.4048682.

Magzoub, M.I., Salehi, S., Hussein, I.A., Nasser, M.S., 2020. Loss circulation in drilling and well construction: the significance of applications of crosslinked polymers in wellbore strengthening: a review. J. Petrol. Sci. Eng. https://doi.org/10.1016/j.petrol.2019.106653.

Mahmoud, H., Hamza, A., Nasser, M.S., Hussein, I.A., Ahmed, R., Karami, H., 2020. Hole cleaning and drilling fluid sweeps in horizontal and deviated wells: comprehensive review. J. Petrol. Sci. Eng. https://doi.org/10.1016/j.petrol.2019.106748.

Mansour, A., Dahi Taleghani, A., Salehi, S., Li, G., Ezeakacha, C., 2019. Smart lost circulation materials for productive zones. J. Pet. Explor. Prod. Technol. 9, 281–296. https://doi.org/10.1007/s13202-018-0458-z.

Mansour, A.K., Taleghani, A.D., Li, G., 2018. Smart Expandable LCMs - A Theoretical and Experimental Study.

Mansour, A.K., Taleghani, A.D., Li, G., 2017. Smart lost circulation materials for wellbore strengthening. In: The 51st U.S. Rock Mechanics/Geomechanics Symposium. OnePetro, San Francisco, California, USA.

Mansure, A.J., 2002. Polyurethane grouting geothermal lost circulation zones. In: Proceedings of the Drilling Conference. Society of Petroleum Engineers (SPE), pp. 659–669. https://doi.org/10.2118/74556-ms.

Mather, P.T., Luo, X., Rousseau, I.A., 2009. Shape memory polymer research. Annu. Rev. Mater. Res. 39, 445–471. https://doi.org/10.1146/annurev-matsci-082908-145419.

Meng, H., Li, G., 2013. A review of stimuli-responsive shape memory polymer composites. Polymer 54, 2199–2221. https://doi.org/10.1016/j.polymer.2013.02.023.

Miyazaki, K., Ohno, T., Karasawa, H., Imaizumi, H., 2019. Performance of polycrystalline diamond compact bit based on laboratory tests assuming geothermal well drilling. Geothermics 80, 185–194. https://doi.org/10.1016/j.geothermics.2019.03.006.

Mohamed, A., Salehi, S., Ahmed, R., 2021a. Significance and complications of drilling fluid rheology in geothermal drilling: a review. Geothermics 93, 102066. https://doi.org/10.1016/j.geothermics.2021.102066.

Mohamed, A., Salehi, S., Ahmed, R., 2021b. Rheological properties of drilling fluids containing special additives for geothermal drilling applications. In: 46th Workshop on Geothermal Reservoir Engineering. Stanford, California, USA, pp. 1–10.

Olasolo, P., Juárez, M.C., Olasolo, J., Morales, M.P., Valdani, D., 2016. Economic analysis of Enhanced Geothermal Systems (EGS). A review of software packages for estimating and simulating costs. Appl. Therm. Eng. 104, 647–658. https://doi.org/10.1016/j.applthermaleng.2016.05.073.

Ravi, K., Savery, M., Reddy, B.R., Whitfill, D., 2006. Cementing technology for low fracture gradient and controlling loss circulation. In: SPE/IADC INDIAN Drilling Technology Conference and Exhibition. Society of Petroleum Engineers, Mumbai, India. https://doi.org/10.2523/102074-ms.

Salehi, S., Nygaard, R., 2011. Evaluation of new drilling approach for widening operational window: implications for wellbore strengthening. In: SPE Production and Operations Symposium, Proceedings. Society of Petroleum Engineers (SPE), pp. 118–133. https://doi.org/10.2118/140753-ms.

Shadravan, A., Amani, M., 2012. HPHT 101-what petroleum engineers and geoscientists should know about high pressure high temperature wells environment. Energy Sci. Technol. 4, 36–60. https://doi.org/10.3968/j.est.1923847920120402.635.

Tare, U.A., Whitfill, D.L., Mody, F.K., 2001. Drilling fluid losses and gains: case histories and practical solutions. In: SPE Annual Technical Conference and Exhibition. Society of Petroleum Engineers, New Orleans, Louisiana, USA, pp. 473–480. https://doi.org/10.2118/71368-ms.

Teodoriu, C., 2015. Why and when does casing fail in geothermal wells. In: Proceedings World Geothermal Congress. Melbourne, Australia.

Vivas, C., Salehi, S., Tuttle, J.D., Rickard, B., 2020. Challenges and opportunities of geothermal drilling for renewable energy generation. Trans. Geoth. Resour. Counc. 44, 904–918.

Vollmar, D., Wittig, V., Bracke, R., 2013. Geothermal Drilling Best Practices : the Geothermal Translation of Conventional Drilling Recommendations - Main Potential Challenges.

Wagle, V., Kalgaonkar, R., Al-Yami, A.S., 2018. Nanoparticle-based chemical treatment for preventing loss circulation. In: SPE Kingdom of Saudi Arabia Annual Technical Symposium and Exhibition 2018. Society of Petroleum Engineers, Dammam, Saudi Arabia. https://doi.org/10.2118/192309-ms.

Wastu, A.R.R., Hamid, A., Samsol, S., 2019. The effect of drilling mud on hole cleaning in oil and gas industry. J. Phys. Conf. Ser. 1402 https://doi.org/10.1088/1742-6596/1402/2/022054.

Werner, B., 2018. The Influence of Drilling Fluid Rheology on Cuttings Bed Behavior. Norwegian University of Science and Technology. https://doi.org/10.13140/RG.2.2.19105.30566.

Whitfill, D., 2008. Lost circulation material selection, particle size distribution and fracture modeling with fracture simulation software. In: IADC/SPE Asia Pacific Drilling Technology Conference. Society of Petroleum Engineers, Jakarta, Indonesia, pp. 382–393. https://doi.org/10.2118/115039-ms.

Wu, Y.-S., 2016. I. Mmiscible Displacement of Non-newtonian Fluids, in: Multiphase Fluid Flow in Porous and Fractured Reservoirs. Elsevier, pp. 127–166. https://doi.org/10.1016/b978-0-12-803848-2.00007-6.

Wu, Y., Patel, H.R., Salehi, S., 2020. Thermal considerations of cement integrity in geothermal wells. In: The 45th Workshop on Geothermal Reservoir Engineering. Stanford, California, USA.

Yakacki, C.M., Shandas, R., Lanning, C., Rech, B., Eckstein, A., Gall, K., 2007. Unconstrained recovery characterization of shape-memory polymer networks for cardiovascular applications. Biomaterials 28, 2255–2263. https://doi.org/10.1016/j.biomaterials.2007.01.030.